

Multi-Scale Video Frame-Synthesis Network with Transitive Consistency Loss

Zhe Hu
Hikvision

zhe.hu@hikvision.com

Yinglan Ma
Adobe

yingma@adobe.com

Lizhuang Ma
East China Normal University

lzma@sei.ecnu.edu.cn

Abstract

Traditional approaches to interpolating/extrapolating frames in a video sequence require accurate pixel correspondences between images, e.g., using optical flow. Their results stem on the accuracy of optical flow estimation, and would generate heavy artifacts when flow estimation failed. Recent methods using auto-encoder have shown impressive progress, however they are usually trained for specific interpolation/extrapolation settings and lack of flexibility and generality for more applications. Moreover, these models are usually heavy in terms of model size which constrains applications on mobile devices. In order to reduce these limitations, we propose a unified network to parameterize the interest frame position and therefore infer interpolated/extrapolated frames within the same framework. To better regularize the network, we introduce a transitive consistency loss and train the network with adversarial training. We adopt a multi-scale structure for the network so that the parameters can be shared across multi-layers. Our approach avoids expensive global optimization of optical flow methods, and is efficient and flexible for video interpolation/extrapolation applications. Experimental results have shown that our method performs favorably against state-of-the-art methods.

1. Introduction

Video frame synthesis, including interpolation and extrapolation, is a classic problem in computer vision and has attracted much interest recently due to the trend of unsupervised/self-supervised learning of video representation. Frame interpolation has been used in numerous applications such as temporal upsampling, frame rate conversion and view synthesis. Frame extrapolation, on the other hand, is related to predicting motion and it is a critical problem for learning interaction with the physical world, e.g., robots, autonomous driving of cars and drones.

Video frame synthesis itself is a challenging problem in the exist of moving deformable objects, object occlusion, illumination change, camera movement, and etc.. Tradi-

tional solutions to frame synthesis first compute dense correspondences, mostly optical flow, and then render image via correspondence-based image warping. Such methods heavily rely on computationally expensive global optimization, due to inherent ambiguities in computing correspondences.

To avoid explicit estimation of dense correspondences, recent methods formulate frame interpolation [31, 32] or extrapolation [9, 42, 5] as a convolution process and estimate the convolution using the neural networks. To speed up the convolution process with spatially-varying kernels, a spatially-adaptive separable convolution approach has been presented for video frame interpolation [32], and obtain impressive interpolation results. However, they still pose the correspondence estimation as a separate step for the video interpolation process.

Most of the work that bypass correspondence estimation treat interpolation problem alone or extrapolation problem alone in a specific setting, e.g., interpolating the frame right in the middle of two input frames, extrapolating next frame with a certain interval. This is because existing networks are specifically designed for a fixed temporal position prediction, and lacks of generality and flexibility. In fact, if we consider a continuous sequence of video frames in temporal domain, either interpolating or extrapolating frames based on a subset of frames can be viewed as a unified problem that predicts frames at certain positions, and therefore should be handled as a whole. This is naturally solved in optical-flow-based methods, in which interpolation/extrapolation are handled along flow directions. Thus, how to elegantly formulate and solve the problem with a unified neural network becomes a critical problem.

In this work, we propose a unified end-to-end network for frame synthesize (interpolate/extrapolate) by parameterizing the temporal position of the interest frame. We propose the Multi-Scale Frame-Synthesis Network (MSFSN) to progressively reconstruct interest frames in a coarse-to-fine manner. The proposed network is able to infer both interpolated and extrapolated frames at any given position with one single model. To achieve this, we introduce a transitive consistency loss to regularize the network for both

interpolation and extrapolation tasks. Adversarial training is used for facilitating the training process. Experimental results show that our network is smaller than autoencoder based methods, e.g., [31, 32, 24], while generating comparable reconstruction accuracy. Our network architecture naturally enables parameters sharing across pyramid levels, since different pyramid levels share the same input/output format and purpose. By sharing parameters across levels, we obtain a compact and flexible model that more levels can be stacked during test to accommodate higher capacity of deeper networks.

2. Related Work

The proposed frame-synthesis GAN aims on interpolating/extrapolating video frames with a unified framework. We adopt a transitive consistency loss for leveraging the problems. Thus, we focus on reviewing work that are relevant to our problem and approach.

Video frame interpolation/extrapolation Video frame interpolation is a classic topic in computer vision and video processing. Traditional frame interpolation methods estimate dense correspondence, mostly optical flow, between input frames and then interpolate one or more intermediate frames by warping the input images [1, 41]. The performance of these methods heavily stem on estimation accuracy of optical flow and require special processing to reduce artifacts. Other than optical flow, approaches along view synthesis perspective have been explored [45, 26]. Meyer et al. [29] developed a phase-based interpolation method that represents motion in the format of pixel phase shift and therefore render intermediate frames by modifying pixel phase. This phase-based method often produces impressive interpolation results, but could fail to preserve high-frequency details under large temporal changes.

Recent approaches formulate frame interpolation/extrapolation with a single convolution step that combines motion estimation and frame synthesis [42, 5, 32, 31, 9]. These methods generate impressive results by estimating spatially-varying kernels within the network and convolve them with input frames to synthesize a new frame. Since these methods involves heavy convolution with large spatially variant kernels, they suffer from high computational load and memory for high-resolution videos. Niklaus et al. [32] propose a method to speed up the final convolution process via approximating 2D kernels with separable 1D kernel, and could process 1080p videos in one pass. Recently, an approach has been proposed to output dense voxel flows through a network and use them to generate interpolated frames [24]. The generated 3D voxel flows encode the motion variance in temporal domain and generate intermediate frames via trilinear interpolation.

Image reconstruction Our work is also inspired by the recent progress of network methods in image enhancement

and reconstruction [10, 18, 23, 4, 7, 21, 20, 30, 8]. Pixel-wise loss functions such as MSE struggle to reconstruct high-frequency details, and therefore minimizing MSE usually lead to over-smooth results [27, 18]. Feature s extracted from a pre-trained VGG network instead of per-pixel error has been proposed to render visually pleasing images [3, 18]. And perceptually more realistic results can be obtained via combining those with generative adversarial networks (GANs) [12] for image generation tasks [43, 27, 22].

Transitive property Transitive property is a property of equivalence, and it has been used to regularize structured data for a long time in the literature. Forward-backward consistency check has proved to be efficient in depth estimation [15] and optical flow [40]. Language translation can also be improved via consistency check with back translation [2, 13]. More recently, higher-order cycle consistency has been used in image-to-image translation [44]. In this work, we are introducing a transitive consistency loss to facilitate training process for video representation.

3. Frame-Synthesis Generative Adversarial Network

Our goal is to learn a mapping function $G : S \times S \times T \rightarrow S$ in image domain S and time domain T , for frame interpolation/extrapolation. We denote a triplet (x_{t_1}, x_{t_2}, t_p) , where $x_{t_i} \in S$, $i = 1, 2$ represents a video frame at timestamp t_i , and t_p is the timestamp of our interest frame. Without loss of generality, we assume $t_1 < t_2$. We denote video frame distribution as $x_t \sim p_{data}$. The mapping predicts the interest frame $y_{t_p} = G(x_{t_1}, x_{t_2}, t_p)$ at timestamp t_p , and $y_{t_p} \in S$. If $t_1 < t_p < t_2$, the problem is a frame interpolation problem. If $t_p < t_1$ or $t_p > t_2$, the problem becomes a frame extrapolation problem.

3.1. Network Architecture

We construct our network using a multi-scale structure [6, 33, 20] as shown in Figure 1. Each level is a sub-network consisting of D residual blocks [14]. We adopt a modified residual block by removing batch normalizations. We will discuss the effect of the block number in Section 4.

Our model takes a triplet (x_{t_1}, x_{t_2}, t_p) as input and progressively predicts the interpolated/extrapolated frames from coarse levels to fine levels. Let S and $y_{t_p}^s$ represent number of pyramid levels and the predicted frame at level s , $s \in \{1, 2, \dots, S\}$ (from coarse to fine, level S is the final reconstruction level). Let x_{t_1} and x_{t_2} be $m \times n$ images that are multiples of 2^{S-1} .

At each pyramid level s , we feed downsampled frames $x_{t_1}^s, x_{t_2}^s$ of size $m/2^{S-s} \times n/2^{S-s}$ and an initial interpolated/extrapolated image $y_{t_p}^{s-1} \uparrow$ upsampled from previous level. We predict the frame $y_{t_p}^s$ at level s by passing input

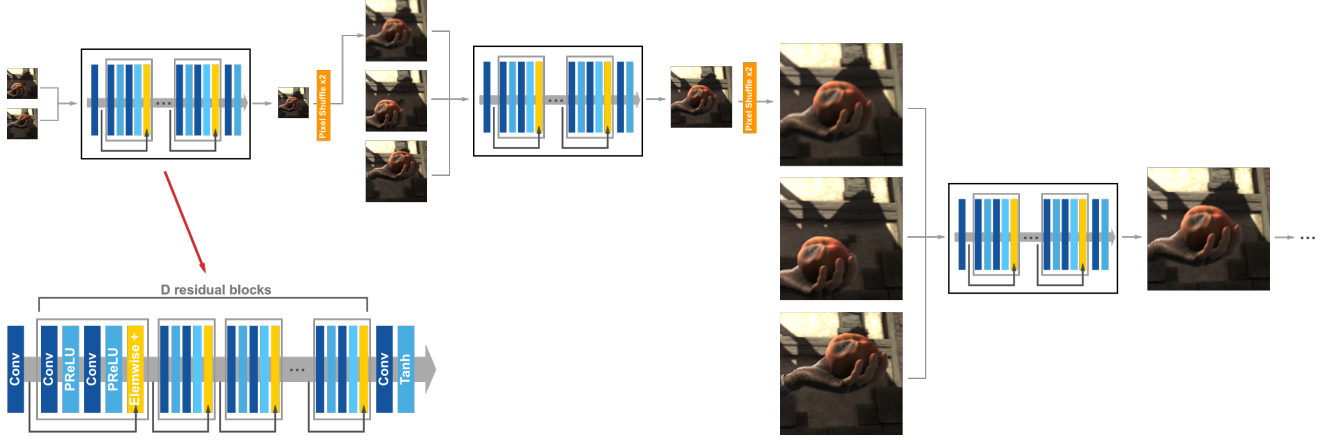


Figure 1. Example of our multi-scale network. Each level is a sub-network consisting of D residual blocks [14] as shown in left bottom. Parameters are shared across pyramid levels, since different pyramid levels (except the coarsest level) share the same input/output format and purpose. We only show a network with 3 pyramid levels for simplicity.

triplet $(x_{t_1}^s, x_{t_2}^s, y_{t_p}^{s-1} \uparrow)$ through our sub-network. In this work, we use a multi-scale structure of 4 levels and 3 sub-networks $\{N_s\}_{s=2}^4$ are $N_s : (x_{t_1}^s, x_{t_2}^s, y_{t_p}^{s-1} \uparrow) = y_{t_p}^s$. The sub-network at coarsest level $s = 1$ takes $(x_{t_1}^1, x_{t_2}^1)$ as input, and is denoted as $N_1 : (x_{t_1}^1, x_{t_2}^1) = y_{t_p}^1$.

Parameter sharing across pyramid levels The entire network is a cascade of sub-networks with same structure at levels except the coarsest level 1. We propose to share the network parameters across those pyramid levels because the network at these levels share same structure and task (i.e., predicting the interest frames with a lower-resolution version as input). As shown in Figure 1, we share the parameters of the sub-networks across all the pyramid levels. As a result, the number of network parameters is independent of the number of levels. We can use one single set of parameters to predict large motion by increasing the number of pyramid levels and this is discussed in Section 4.

3.2. Loss Function

Considering the supreme benefit of adversarial training on synthesizing realistic texture [21, 44], we formulate our model in a GAN framework. For the mapping function G , we introduce an adversarial discriminator D , where D aims to distinguish between images and generated images by G [12]. Our objective contains four terms: 1) pixel reconstruction loss; 2) feature reconstruction loss to encourage similarity in feature representation; 3) adversarial losses for matching the distribution of generated images to the data distribution in the target feature domain; 4) transitive consistency losses to enhance the mapping function G with more constraints.

Pixel reconstruction loss We adopt a per-pixel differ-

ence loss in ℓ_1 norm as

$$\mathcal{L}_{pix}(G) = \mathbb{E}_{p_{data}} [|\phi(G(x_{t_1}, x_{t_2}, t_p)) - \phi(y_{t_p})|_1], \quad (1)$$

which is also suggested in [39, 32] to reduce blur effect rather than ℓ_2 norm.

Feature reconstruction loss Inspired by perceptual loss functions used in image reconstruction and style transfer networks [10, 8, 18], we use a feature reconstruction loss:

$$\mathcal{L}_{feat}(G) = \mathbb{E}_{p_{data}} [|\phi(G(x_{t_1}, x_{t_2}, t_p)) - \phi(y_{t_p})|_2]. \quad (2)$$

This loss is to encourage the feature of the output image to match that of the target image, and we use a similar loss network ϕ as [10, 18] based on 16-layer VGG network [37] pretrained on ImageNet [35].

Adversarial loss We apply adversarial losses [12] to the mapping function G and its discriminator D as:

$$\begin{aligned} \mathcal{L}_{GAN}(G, D) &= \mathbb{E}_{p_{data}} [\log_{x_{t_p}} D(x_{t_p})] \\ &+ \mathbb{E}_{p_{data}} [\log(1 - D(G(x_{t_1}, x_{t_2}, t_p)))], \end{aligned} \quad (3)$$

where G tries to generate image $G(x_{t_1}, x_{t_2}, t_p)$ that looks similar to the frame x_{t_p} at timestamp t_p , while D aims to distinguish between generated image $G(x_{t_1}, x_{t_2}, t_p)$ and real sample x_{t_p} . In other words, G and D are trained to optimize the objective in a minmax manner.

Adversarial training, in theory, can learn a discriminator D to help the mapping function G that produces outputs identically distributed as target domains S when G is a stochastic function [12]. However, with large enough network capacity, there are countless network with different parameter sets that can map a set of inputs to the target domain, with each of them mapping to a different image in the target domain. Thus, adversarial losses alone cannot guarantee that the learned function maps an input (x_{t_1}, x_{t_2}, t_p) to the desired output x_{t_p} .

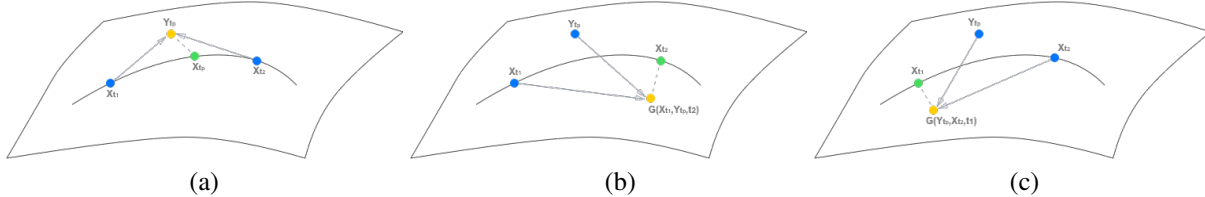


Figure 2. Example of transitive property. We aim to learn the frame synthesis mapping $G : S \times S \times T \rightarrow S$. Let $x_{t_1}, x_{t_2}, x_{t_p}$ denote three frames capturing the same scene in a video, and the mapping $y_{t_p} = G(x_{t_1}, x_{t_2}, t_p)$. The frames should lie on a manifold that represents the images of the scene, specifically a curve in the manifold that represents the frames in the video. To further regularize the mappings, we introduce transitive consistency loss that captures the transitive mappings $G(y_{t_p}, x_{t_2}, t_1) \approx x_{t_1}$ and $G(x_{t_1}, y_{t_p}, t_2) \approx x_{t_2}$.

Transitive consistency loss To further regularize the mapping function, we argue that the learned mapping function for frame interpolation/extrapolation should be transitive-consistent: given a mapping $y_{t_p} = G(x_{t_1}, x_{t_2}, t_p)$, we should have transitive mappings for x_{t_1} and x_{t_2} giving y_{t_p} as an input,

$$\begin{aligned} G(y_{t_p}, x_{t_2}, t_1) &\approx x_{t_1}, \\ G(x_{t_1}, y_{t_p}, t_2) &\approx x_{t_2}. \end{aligned} \quad (4)$$

We call this *transitive consistency*, and an illustration is shown in Figure 2. Therefore, we can formulate this behavior using a transitive consistency loss:

$$\begin{aligned} \mathcal{L}_{tran}(G) &= \mathbb{E}_{p_{data}}[|G(x_{t_1}, y_{t_p}, t_2) - x_{t_2}|_1] \\ &+ \mathbb{E}_{p_{data}}[|G(y_{t_p}, x_{t_2}, t_1) - x_{t_1}|_1]. \end{aligned} \quad (5)$$

In preliminary experiments, we also tried replacing the ℓ_1 norm in this loss with an ℓ_2 , but did not observe improved performance.

The behavior induced by the cycle consistency loss can be observed in Figure 4: the reconstructed images end up matching closely to the input images x .

Objective function By combining adversarial loss and transitive consistency loss, our final objective function becomes:

$$\begin{aligned} \mathcal{L}(G, D) &= \mathcal{L}_{pix}(G) + \lambda_{feat} \mathcal{L}_{feat}(G) \\ &+ \lambda_{GAN} \mathcal{L}_{GAN}(G, D) + \lambda_{tran} \mathcal{L}_{tran}(G), \end{aligned} \quad (6)$$

where λ_* are the weights to balance different components. Thus, our goal is to solve:

$$(G^*, D^*) = \arg \min_G \max_D \mathcal{L}(G, D) \quad (7)$$

In Section 4, we compare our method of the full objective, against ablations of the transitive consistency loss \mathcal{L}_{tran} , and show that transitive consistency loss plays a critical role in obtaining high-quality results.

3.3. Implementation and Training Details

In practice, instead of feeding the time stamp t_p directly for mapping $G(x_{t_1}, x_{t_2}, t_p)$, we feed a ratio $r_p(t_1, t_2) =$

$(t_p - t_1)/(t_2 - t_1)$ representing the relative temporal position comparing to t_1 and t_2 . Similarly, temporal ratios $(t_1 - t_p)/(t_2 - t_p)$ and $(t_2 - t_1)/(t_p - t_1)$ are used for mappings $G(y_{t_p}, x_{t_2}, t_1)$ and $G(x_{t_1}, y_{t_p}, t_2)$ respectively.

In the proposed MSFSN, all convolutional layers have 64 filters with the size of 5×5 , and they are initialized using the Xavier initialization [11]. We use the pixel-shuffle technique [36] in the upsampling layer. We use the leaky rectified linear units (LReLU) [25] with a negative slope of 0.2 as the non-linear activation function. For loss function, we set $\lambda_{feat} = 2e - 5$, $\lambda_{GAN} = 5e - 2$, and $\lambda_{tran} = 0.2$.

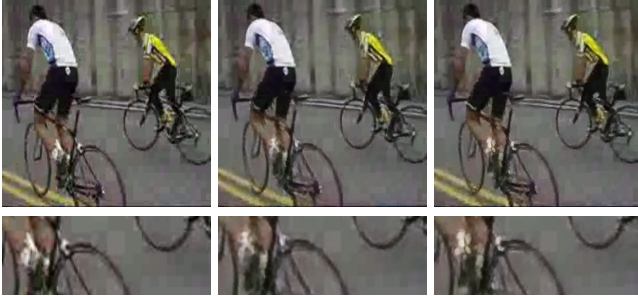
The networks are trained using Adam optimization [19] with $\beta_1 = 0.9$ and $\beta_2 = 0.999$. We use a batch size of 8, a patch size of 128 and 200 iterations per epoch for training. At each pass, three nearby frames are sampled from the videos with randomly selected intervals. To guarantee that each training data contains enough information, we rule out smooth patches based on variance. We use a learning rate of $1e - 4$ for the initial generator training and decay it during the adversarial training until the network converges. All our networks are trained on a single Nvidia P40 GPU.

We include various types of data augmentation during training: 1) randomly rotate images by $\{0, 90, 180, 270\}$ degrees; 2) randomly flip images horizontally or vertically; 3) randomly crop patches of the same resolution of the training input; 4) adding additive Gaussian noise sampled uniformly from $N(0, 0.1)$. During test, images are padded with mirror reflection such that their sizes are multiples of 2^{S-1} .

4. Model Analysis

In this section, we first validate the contributions of different components of the proposed network at an interpolation ratio 0.5 (interpolating middle in-between frame). We then discuss the effect of multiple in-between frame interpolation.

For validation experiments, we use the GOPRO dataset [30], in which the videos are captured using a GOPRO camera at 240 fps. Since the videos are captured under significant camera movement, object motion and illumination change at a high sampling rate, the dataset well fits



(a) Ground truth (b) Ours-Gen (c) Ours

Figure 3. Example of frame interpolation on UCF-101 dataset [38]. We compare the proposed network with that trained without adversarial training (Ours-Gen).

our purpose. We split GOPRO dataset into training/test sets (2103/1111 frames) and train our model on the training set while evaluating on test set.

Adversarial training To validate the influence of the adversarial training, we train the proposed model with only generator (Ours-Gen) and compare it with the original model with the adversarial discriminator. We test this using the setting described in Section 5 and show results in Table 3. The proposed model does not outperform Ours-Gen in PSNR, but is able to render visually pleasing images. As shown in Figure 4, our proposed method generate sharper images but the corresponding PSNR is slightly lower than those from Ours-Gen. We note that our method removes some artifacts existed in the input images, e.g., the blocky artifacts in the example, thus is at a disadvantage in quantitative comparison.

Pyramid depth Since the sub-networks in our model share same parameters, we can easily apply different numbers of pyramid levels during test with one trained model. We train our model of 4 pyramid levels on GOPRO training set and test the performance of different numbers of pyramid levels on GOPRO test dataset. Moreover, we evaluate the results on different intervals: 1/2/3 frame intervals, meaning that the temporal distances between the interpolated frames and the pairs of input frames are 1/2/3 frames. The quantitative results are shown in Table 1. As shown in the table, stacking more levels in general leads to better performance (exception is 4-level structure with which the model is trained), and it does not gain improvement after 6-level structure on the dataset. This is because long-range motion can be better handled by delving into lower down-sampled images.

Sub-network depth Each of the sub-network contains D residual blocks and we explore the performance influence on the sub-network depth, i.e., number of residual blocks. We train the proposed model of 4 pyramid levels with different depth, $D = 5, 9, 12, 16$ at each level, and show the

Pyramid depth/ Time interval	GOPRO (PSNR/SSIM)		
	1 frame	2 frames	3 frames
3 levels	32.56/0.90	31.98/0.88	31.39/0.81
4 levels	34.76/0.91	34.24/0.90	33.56/0.85
5 levels	34.25/0.91	33.71/0.90	33.04/0.84
6 levels	34.58/0.91	34.04/0.90	33.35/0.84
7 levels	34.46/0.91	33.91/0.90	33.21/0.84

Table 1. Quantitative evaluation on the number of pyramid levels. We train the model of 4 pyramid levels on GOPRO training set [30] and evaluate the performance of different numbers of pyramid levels on GOPRO test set. The results are evaluated for frame interpolation at 1/2/3 frame intervals.

Network depth/ Time interval	#Parameters	GOPRO (PSNR/SSIM)		
		1 frame	2 frames	3 frames
5	4,140,633	34.43/0.90	33.82/0.88	33.13/0.81
9	7,419,481	34.76/0.91	34.24/0.90	33.56/0.85
12	9,878,617	34.79/0.90	34.26/0.90	33.65/0.85
16	13,157,465	34.66/0.89	34.14/0.90	33.42/0.84

Table 2. Quantitative evaluation on the sub-network depth at each level. We build MSFSN with different sub-network depth by varying the numbers of residual blocks. The results are evaluated for frame interpolation task on the UCF-101 dataset [38].

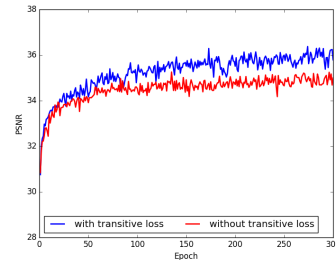


Figure 4. Training curves with/without transitive consistency loss in terms of PSNR value. We show the first 300 epochs for better visualization.

performance on interpolation task in Table 2. The models are trained on GOPRO training set and evaluated on GOPRO test dataset.

In general, deeper networks perform better than shallower ones at the expense of increased training time and computational cost. The network with $D = 16$ does not perform well in terms of PSNR, and the reason could be that the network with large capacity is easy to fall into a local minimum. We use $D = 9$ in our model for most of our experiments to compromise between performance and speed.

Loss function To validate the effectiveness of the transitive consistency loss function, we compare with the proposed network without the transitive consistency loss function. We show the training curve in terms of PSNR metric instead of loss curve, as the loss function has been changed when removing transitive consistency loss. As illustrated in

Method	UCF-101		THUMOS-15	
	PSNR	SSIM	PSNR	SSIM
BeyondMSE	32.8	0.93	32.3	0.91
EpicFlow	34.2	0.95	33.9	0.94
FlowNet2	34.0	0.94	33.8	0.94
DVF	35.8	0.96	35.4	0.95
AdapSC	36.2	0.95	36.4	0.96
Ours-Gen	35.9	0.96	35.3	0.95
Ours	35.7	0.95	35.1	0.95

Table 3. Performance (PSNR and SSIM) of video frame interpolation on UCF-101 and THUMOS-15 datasets.

Figure 4, the transitive consistency loss facilitates network training and improves the reconstruction results.

5. Experimental Results

In this section, we compare the proposed MSFSN with several state-of-the-art methods on benchmark datasets. We present the quantitative and qualitative comparison in terms of interpolation and extrapolation. Finally, we discuss the limitation of the proposed method. For the experiments in this section, we train our model on UCF-101 training dataset.

5.1. Interpolation

We compare our approach against several methods, including optical flow techniques: EpicFlow [34] and FlowNet2 [17]; and frame synthesis methods: BeyondMSE [27], DVF [24] and AdapSC [32]. We carry out extensive experiments on public benchmark datasets: UCF-101 [38] and THUMOS-15 [16]. UCF-101 and THUMOS-15 contain videos with object motions in relatively low resolution. To synthesize the interpolated images given the estimated flow fields, we apply the interpolation algorithm used in the Middlebury interpolation benchmark [1].

As shown in Figure 8, the correspondence-based methods would generate images with ringing or blurry artifact on the regions where correspondence estimation fails, e.g., front of motor boat, while our network is able to render pleasing results. We present quantitative comparisons on the benchmark datasets in Table 3. Our approach performs better than flow-based methods EpicFlow [34] and FlowNet2 [17], and comparable to frame synthesis network DVF [24]. The method AdapSC [32] usually generate sharper results than our results, due to their correspondence nature via local filtering. That is, when the correspondences/spatially-varying kernels are accurately estimated, they can generate sharp results as the input images.

Interpolating multiple frames Unlike those networks trained on specific interpolation settings, e.g., interpolating middle in-between frame, our method is capable of synthe-

Method	UCF-101		THUMOS-15	
	PSNR	SSIM	PSNR	SSIM
BeyondMSE	30.6	0.90	30.2	0.89
EpicFlow	31.3	0.92	31.0	0.92
FlowNet2	31.8	0.92	31.7	0.92
DVF	32.7	0.93	32.2	0.92
Ours-Gen	32.5	0.92	32.1	0.92
Ours	32.2	0.92	31.8	0.92

Table 4. Performance (PSNR and SSIM) of video frame prediction on UCF-101 and THUMOS-15 datasets.

sizing frames at any in-between position, without computing correspondences. We show comparison with flow-based method [17] and frame interpolation network [32] on interpolating multiple in-between frames. To compare with the network [32] which can only interpolate middle in-between frame, we evaluate on the scenario of interpolating three equally spaced frames. In this case, we obtain their results by two-stage interpolation, which is first interpolating middle frame and then interpolating the other two using the middle frame as an input. As shown in Figure 6, our method renders sharp results while maintains the straight road lines while others cannot.

User study To better understand the visual quality of different methods, we conducted a user study on the interpolated frames. We develop a web-based system to display and collect study results. The system provides two side-by-side results at a time, one from our method and the other from a randomly selected method. Each pair of results is randomly selected and placed. The results show that our method is preferred or comparable to state-of-the-art methods [34, 17, 32]. Due to space limitation, we put the user study results in the supplementary material.

5.2. Extrapolation

The trained model can be directly applied to video extrapolation tasks without fine tuning. Most of the interpolation networks mentioned are trained for a specific setting, and therefore cannot apply directly to the extrapolation cases. We compare with state-of-the-art methods on UC-101 and THUMOS-15 datasets and present quantitative results in Table 4. Qualitative comparisons are given in Figure 15.

5.3. Limitation and Discussion

While our network is capable to handle large motion, the results from our method are usually more blurry than than corresponding-based method [32], as they fuse corresponding pixels through a local window filtering. We will explore the framework to combine the benefit of corresponding-based method into the unified framework in our future work. Another limitation of the proposed network is that the synthesized frame is assumed to follow the motion momentum,



(a) Ground truth (b) EpicFlow (c) FlowNet2 (d) DVF (e) AdapSC (f) Ours
 Figure 5. Examples of video frame interpolation from UCF-101 dataset [38]. We compare with several state-of-the-art methods, including EpicFlow [34], FlowNet2 [17], DVF [24] and AdapSC [32].



(a) First input frame (b) Interpolated frame 1 (c) Interpolated frame 3 (d) Second input frame
 Figure 6. Example of multiple frame interpolation from KITTI dataset [28]. For this example, we interpolate three equally spaced frames in-between and show comparison with FlowNet2 [17] and AdapSC [32]. The first to third rows are results from FlowNet2, AdapSC and ours respectively. Here we show first and third interpolated frames for comparison.

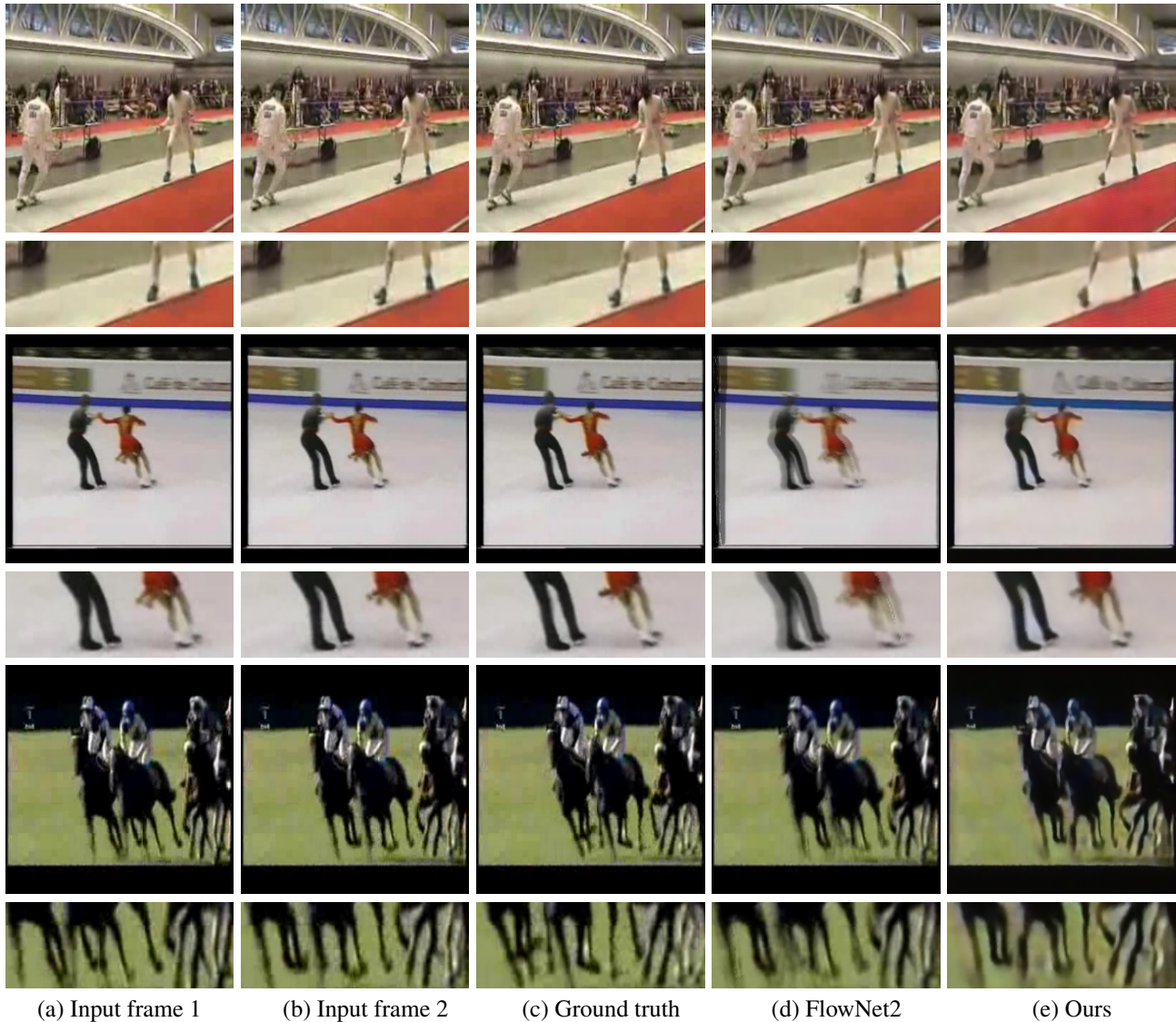


Figure 7. Examples of video frame extrapolation from UCF-101 dataset [38].

which is constrained and parameterized using one temporal variable. How to generalize the motion patterns in the network will also be an interesting research direction.

6. Conclusion

In this paper, we propose a unified deep neural network for video frame synthesis. The proposed model progressively predicts interpolated/extrapolated frames in a coarse-to-fine manner. We introduce a transitive consistency loss to facilitate the network training and enable the network for both interpolation and extrapolation capabilities. By sharing parameters across pyramid levels, the network is compact and is practical to use in devices where memory and computation power are limited. The proposed model

can be easily extend to scenarios, e.g., long-range motion, where deeper pyramid is needed. Extensive evaluations on benchmark datasets demonstrate that the proposed model performs favorably against state-of-the-art algorithms.

References

- [1] S. Baker, D. Scharstein, J. Lewis, S. Roth, M. J. Black, and R. Szeliski. A database and evaluation methodology for optical flow. *International Journal Computer Vision*, 92(1):1–31, 2011. 2, 6
- [2] R. W. Brislin. Back-translation for cross-cultural research. *Journal of cross-cultural psychology*, 1(3):185–216, 1970. 2
- [3] J. Bruna, P. Sprechmann, and Y. LeCun. Super-resolution with deep convolutional sufficient statistics. *arXiv preprint arXiv:1511.05666*, 2015. 2

- [4] H. C. Burger, C. J. Schuler, and S. Harmeling. Image denoising: Can plain neural networks compete with BM3D. In *Proceedings of the IEEE Conference on Computer Vision and Pattern Recognition*, pages 2392–2399. IEEE, 2012. 2
- [5] B. De Brabandere, X. Jia, T. Tuytelaars, and L. Van Gool. Dynamic filter networks. In *Neural Information Processing Systems*, 2016. 1, 2
- [6] E. L. Denton, S. Chintala, R. Fergus, et al. Deep generative image models using a laplacian pyramid of adversarial networks. In *Neural Information Processing Systems*, pages 1486–1494, 2015. 2
- [7] C. Dong, C. C. Loy, K. He, and X. Tang. Image super-resolution using deep convolutional networks. *IEEE Transactions on Pattern Analysis and Machine Intelligence*, 38(2):295–307, 2016. 2
- [8] A. Dosovitskiy and T. Brox. Generating images with perceptual similarity metrics based on deep networks. In *Neural Information Processing Systems*, pages 658–666, 2016. 2, 3
- [9] C. Finn, I. Goodfellow, and S. Levine. Unsupervised learning for physical interaction through video prediction. In *Neural Information Processing Systems*, pages 64–72, 2016. 1, 2
- [10] L. A. Gatys, A. S. Ecker, and M. Bethge. A neural algorithm of artistic style. *arXiv preprint arXiv:1508.06576*, 2015. 2, 3
- [11] X. Glorot and Y. Bengio. Understanding the difficulty of training deep feedforward neural networks. In *Proceedings of the Thirteenth International Conference on Artificial Intelligence and Statistics*, pages 249–256, 2010. 4
- [12] I. Goodfellow, J. Pouget-Abadie, M. Mirza, B. Xu, D. Warde-Farley, S. Ozair, A. Courville, and Y. Bengio. Generative adversarial nets. In *Neural Information Processing Systems*, pages 2672–2680, 2014. 2, 3
- [13] D. He, Y. Xia, T. Qin, L. Wang, N. Yu, T. Liu, and W.-Y. Ma. Dual learning for machine translation. In *Neural Information Processing Systems*, pages 820–828, 2016. 2
- [14] K. He, X. Zhang, S. Ren, and J. Sun. Deep residual learning for image recognition. In *Proceedings of the IEEE Conference on Computer Vision and Pattern Recognition*, pages 770–778, 2016. 2, 3
- [15] H. Hirschmuller. Stereo processing by semiglobal matching and mutual information. *IEEE Transactions on Pattern Analysis and Machine Intelligence*, 30(2):328–341, 2008. 2
- [16] H. Idrees, A. R. Zamir, Y.-G. Jiang, A. Ghorban, I. Laptev, R. Sukthankar, and M. Shah. The THUMOS challenge on action recognition for videos in the wild. *Computer Vision and Image Understanding*, 155:1–23, 2017. 6
- [17] E. Ilg, N. Mayer, T. Saikia, M. Keuper, A. Dosovitskiy, and T. Brox. FlowNet 2.0: Evolution of optical flow estimation with deep networks. *arXiv preprint arXiv:1612.01925*, 2016. 6, 7, 11, 12, 13, 14, 15, 16, 17
- [18] J. Johnson, A. Alahi, and L. Fei-Fei. Perceptual losses for real-time style transfer and super-resolution. In *Proceedings of European Conference on Computer Vision*, pages 694–711. Springer, 2016. 2, 3
- [19] D. Kingma and J. Ba. Adam: A method for stochastic optimization. *arXiv preprint arXiv:1412.6980*, 2014. 4
- [20] W.-S. Lai, J.-B. Huang, N. Ahuja, and M.-H. Yang. Deep laplacian pyramid networks for fast and accurate super-resolution. *arXiv preprint arXiv:1704.03915*, 2017. 2
- [21] C. Ledig, L. Theis, F. Huszár, J. Caballero, A. Cunningham, A. Acosta, A. Aitken, A. Tejani, J. Totz, Z. Wang, et al. Photo-realistic single image super-resolution using a generative adversarial network. *arXiv preprint arXiv:1609.04802*, 2016. 2, 3
- [22] C. Li and M. Wand. Combining markov random fields and convolutional neural networks for image synthesis. In *Proceedings of the IEEE Conference on Computer Vision and Pattern Recognition*, pages 2479–2486, 2016. 2
- [23] C. Li and M. Wand. Precomputed real-time texture synthesis with markovian generative adversarial networks. In *Proceedings of European Conference on Computer Vision*, pages 702–716. Springer, 2016. 2
- [24] Z. Liu, R. Yeh, X. Tang, Y. Liu, and A. Agarwala. Video frame synthesis using deep voxel flow. *arXiv preprint arXiv:1702.02463*, 2017. 2, 6, 7, 11, 12, 13, 14, 15
- [25] A. L. Maas, A. Y. Hannun, and A. Y. Ng. Rectifier nonlinearities improve neural network acoustic models. In *Proceedings of International Conference on Machine Learning*, volume 30, 2013. 4
- [26] D. Mahajan, F.-C. Huang, W. Matusik, R. Ramamoorthi, and P. Belhumeur. Moving gradients: a path-based method for plausible image interpolation. *ACM Transactions on Graphics (TOG)*, 28(3):42, 2009. 2
- [27] M. Mathieu, C. Couprie, and Y. LeCun. Deep multi-scale video prediction beyond mean square error. *arXiv preprint arXiv:1511.05440*, 2015. 2, 6
- [28] M. Menze and A. Geiger. Object scene flow for autonomous vehicles. In *Conference on Computer Vision and Pattern Recognition (CVPR)*, 2015. 7
- [29] S. Meyer, O. Wang, H. Zimmer, M. Grosse, and A. Sorkine-Hornung. Phase-based frame interpolation for video. In *Proceedings of the IEEE Conference on Computer Vision and Pattern Recognition*, pages 1410–1418, 2015. 2
- [30] S. Nah, T. H. Kim, and K. M. Lee. Deep multi-scale convolutional neural network for dynamic scene deblurring. *arXiv preprint arXiv:1612.02177*, 2016. 2, 4, 5, 16, 17
- [31] S. Niklaus, L. Mai, and F. Liu. Video frame interpolation via adaptive convolution. In *Proceedings of the IEEE Conference on Computer Vision and Pattern Recognition*, 2017. 1, 2
- [32] S. Niklaus, L. Mai, and F. Liu. Video frame interpolation via adaptive separable convolution. In *Proceedings of IEEE International Conference on Computer Vision*, 2017. 1, 2, 3, 6, 7, 11, 12, 13, 14, 15, 16, 17
- [33] A. Ranjan and M. J. Black. Optical flow estimation using a spatial pyramid network. *arXiv preprint arXiv:1611.00850*, 2016. 2
- [34] J. Revaud, P. Weinzaepfel, Z. Harchaoui, and C. Schmid. Epicflow: Edge-preserving interpolation of correspondences for optical flow. In *Proceedings of the IEEE Conference on Computer Vision and Pattern Recognition*, pages 1164–1172, 2015. 6, 7, 11, 12, 13, 14, 15

- [35] O. Russakovsky, J. Deng, H. Su, J. Krause, S. Satheesh, S. Ma, Z. Huang, A. Karpathy, A. Khosla, M. Bernstein, et al. Imagenet large scale visual recognition challenge. *International Journal Computer Vision*, 115(3):211–252, 2015. [3](#)
- [36] W. Shi, J. Caballero, F. Huszár, J. Totz, A. P. Aitken, R. Bishop, D. Rueckert, and Z. Wang. Real-time single image and video super-resolution using an efficient sub-pixel convolutional neural network. In *Proceedings of the IEEE Conference on Computer Vision and Pattern Recognition*, pages 1874–1883, 2016. [4](#)
- [37] K. Simonyan and A. Zisserman. Very deep convolutional networks for large-scale image recognition. *arXiv preprint arXiv:1409.1556*, 2014. [3](#)
- [38] K. Soomro, A. R. Zamir, and M. Shah. UCF101: A dataset of 101 human actions classes from videos in the wild. *arXiv preprint arXiv:1212.0402*, 2012. [5](#), [6](#), [7](#), [8](#), [11](#), [12](#), [13](#), [14](#), [15](#), [18](#), [19](#), [20](#)
- [39] N. Srivastava, E. Mansimov, and R. Salakhudinov. Unsupervised learning of video representations using lstms. In *Proceedings of International Conference on Machine Learning*, pages 843–852, 2015. [3](#)
- [40] N. Sundaram, T. Brox, and K. Keutzer. Dense point trajectories by gpu-accelerated large displacement optical flow. In *Proceedings of European Conference on Computer Vision*, pages 438–451. Springer, 2010. [2](#)
- [41] M. Werlberger, T. Pock, M. Unger, and H. Bischof. Optical flow guided tv-l1 video interpolation and restoration. In *EMMCVPR*, pages 273–286. Springer, 2011. [2](#)
- [42] T. Xue, J. Wu, K. L. Bouman, and W. T. Freeman. Visual dynamics: Probabilistic future frame synthesis via cross convolutional networks. In *Neural Information Processing Systems*, 2016. [1](#), [2](#)
- [43] X. Yu and F. Porikli. Ultra-resolving face images by discriminative generative networks. In *Proceedings of European Conference on Computer Vision*, pages 318–333. Springer, 2016. [2](#)
- [44] J.-Y. Zhu, T. Park, P. Isola, and A. A. Efros. Unpaired image-to-image translation using cycle-consistent adversarial networks. *arXiv preprint arXiv:1703.10593*, 2017. [2](#), [3](#)
- [45] C. L. Zitnick, S. B. Kang, M. Uyttendaele, S. Winder, and R. Szeliski. High-quality video view interpolation using a layered representation. In *ACM Transactions on Graphics (TOG)*, volume 23, pages 600–608. ACM, 2004. [2](#)

A. Additional Qualitative Results

We present additional results on frame interpolation, in Figure [8](#), [9](#), [10](#), [11](#), [12](#), [13](#), [14](#), and frame extrapolation, in Figure [15](#), [16](#), [17](#).



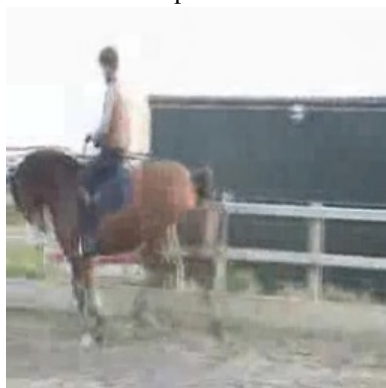
Ground truth

EpicFlow

FlowNet2



DVF



AdapSC



Ours



Ground truth



EpicFlow



FlowNet2



DVF



AdapSC



Ours

Figure 8. Examples of video frame interpolation from UCF-101 dataset [38]. We compare with several state-of-the-art methods, including EpicFlow [34], FlowNet2 [17], DVF [24] and AdapSC [32].

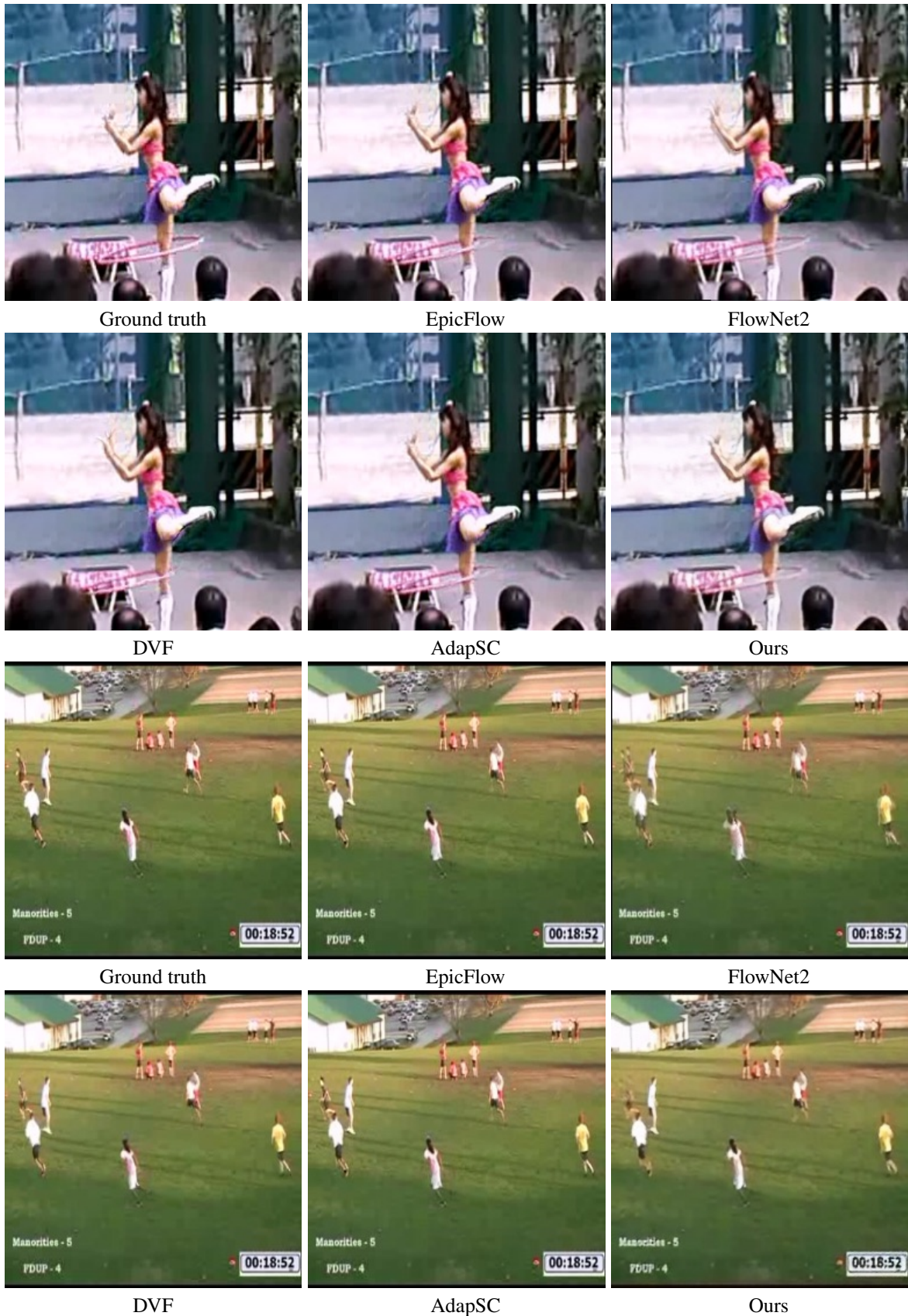


Figure 9. Examples of video frame interpolation from UCF-101 dataset [38]. We compare with several state-of-the-art methods, including EpicFlow [34], FlowNet2 [17], DVF [24] and AdapSC [32].

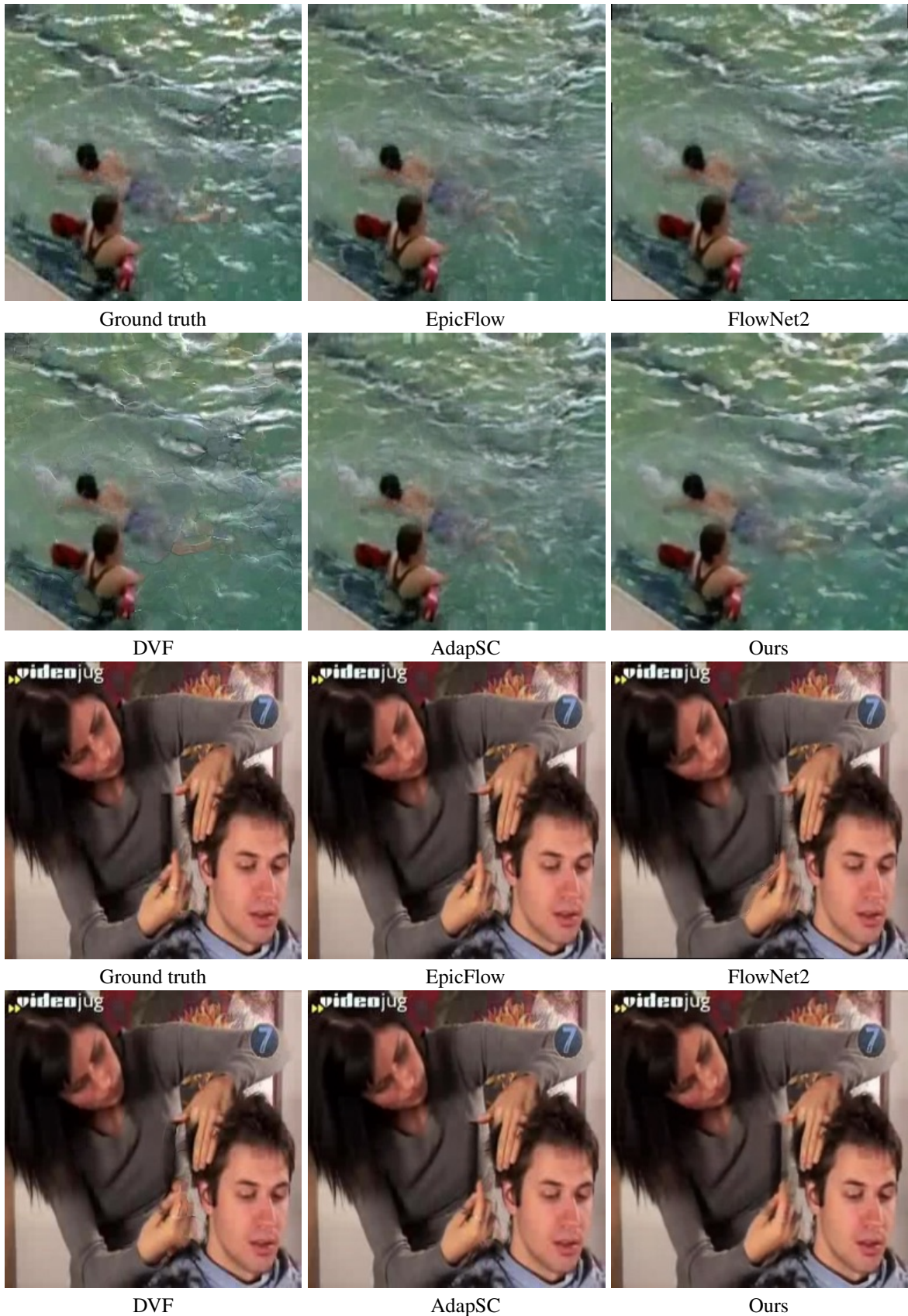


Figure 10. Examples of video frame interpolation from UCF-101 dataset [38]. We compare with several state-of-the-art methods, including EpicFlow [34], FlowNet2 [17], DVF [24] and AdapSC [32].

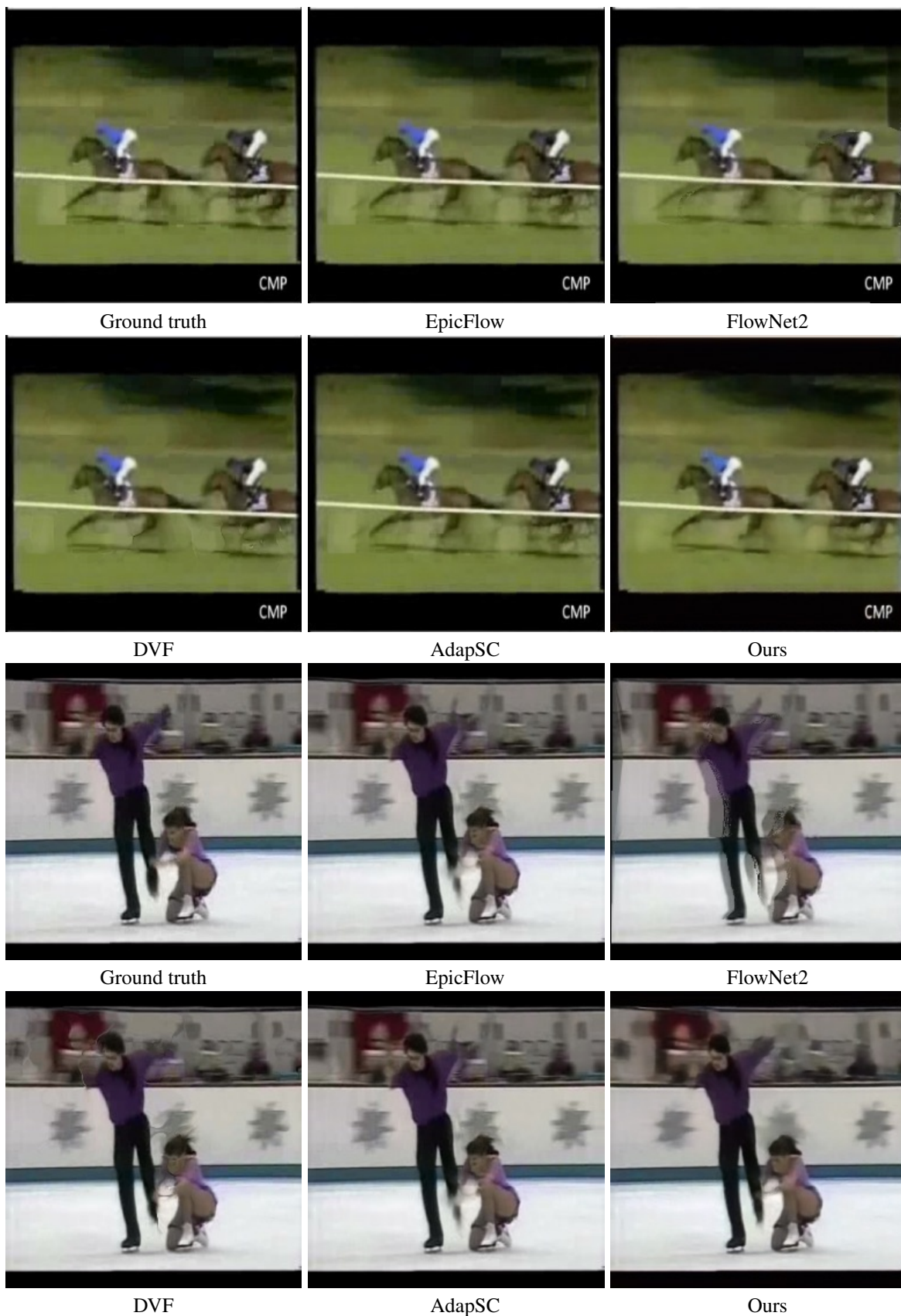


Figure 11. Examples of video frame interpolation from UCF-101 dataset [38]. We compare with several state-of-the-art methods, including EpicFlow [34], FlowNet2 [17], DVF [24] and AdapSC [32].

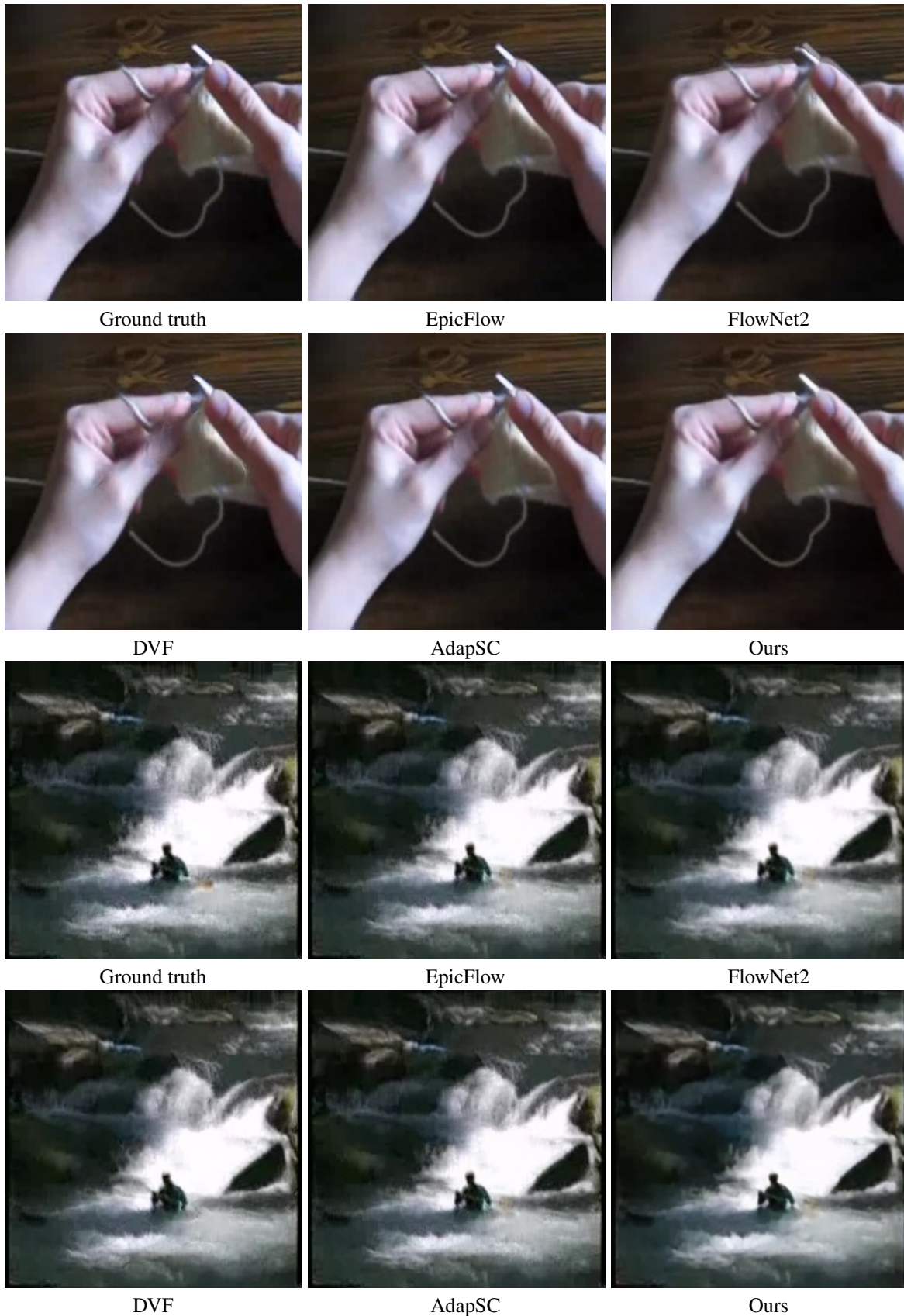


Figure 12. Examples of video frame interpolation from UCF-101 dataset [38]. We compare with several state-of-the-art methods, including EpicFlow [34], FlowNet2 [17], DVF [24] and AdapSC [32].

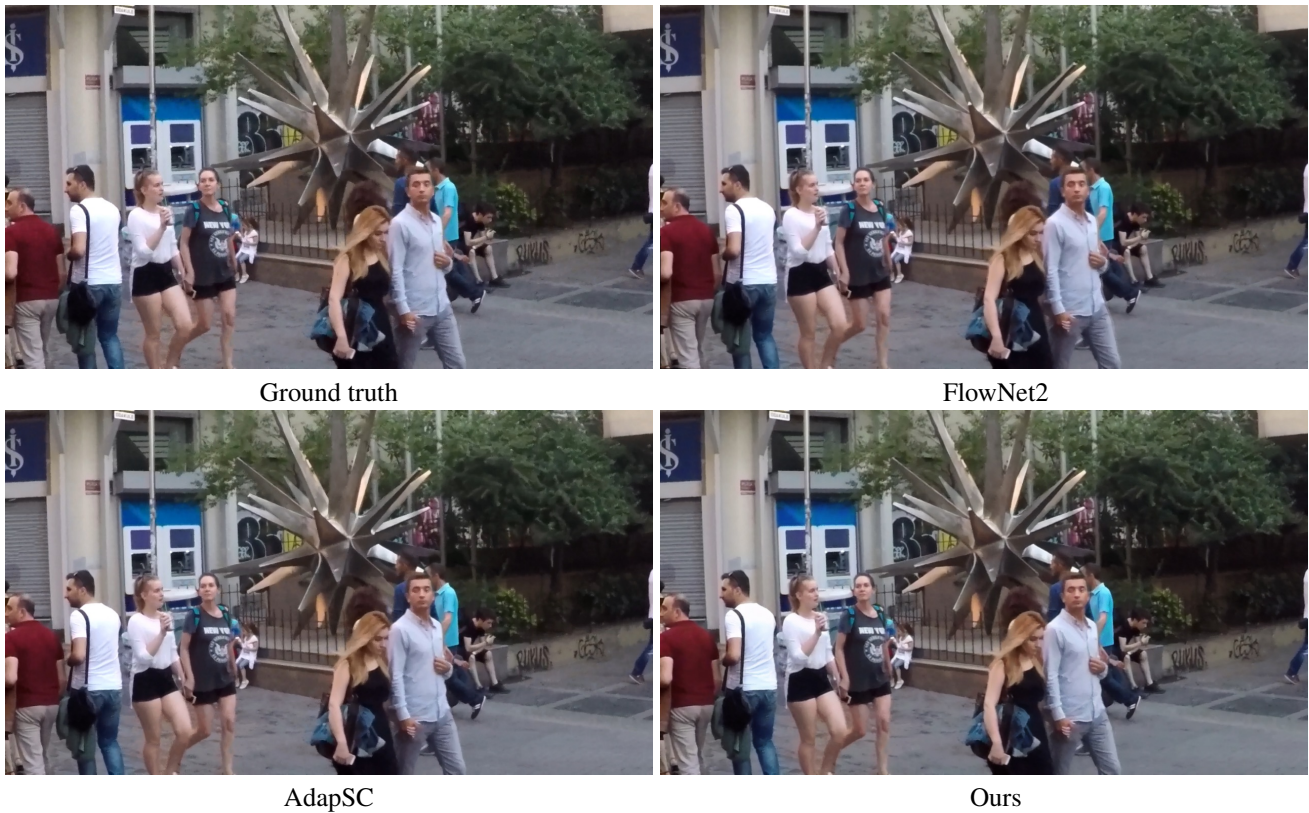


Figure 13. Examples of video frame interpolation from GOPRO test dataset [30]. We compare with two state-of-the-art methods, FlowNet2 [17] and AdapSC [32].

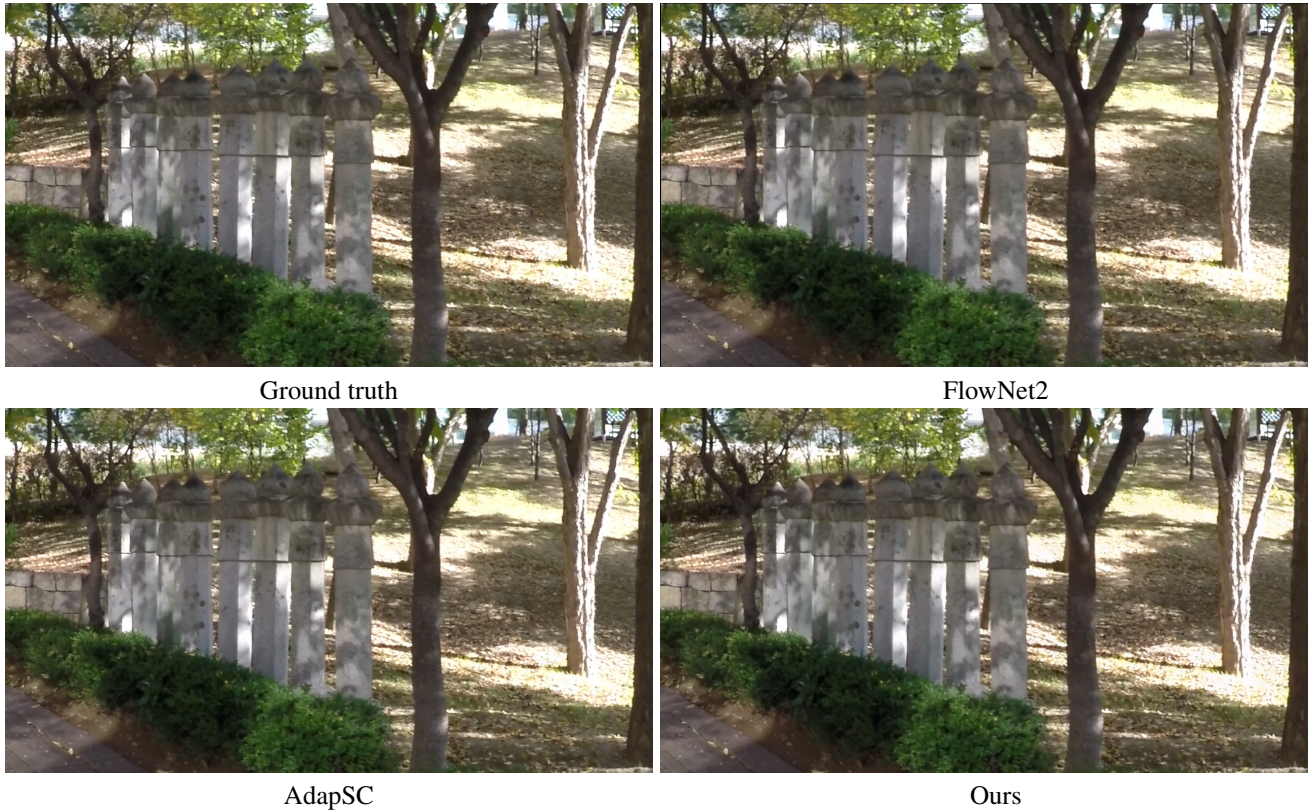


Figure 14. Examples of video frame interpolation from GOPRO test dataset [30]. We compare with two state-of-the-art methods, FlowNet2 [17] and AdapSC [32].



Frame 1

Frame 2

Frame 3 (ground-truth)



FlowNet2



Ours



Frame 1



Frame 2



Frame 3 (ground-truth)



FlowNet2



Ours

Figure 15. Examples of video frame prediction from UCF-101 dataset [38].



Frame 1

Frame 2

Frame 3 (ground-truth)



FlowNet2



Ours



Frame 1



Frame 2



Frame 3 (ground-truth)



FlowNet2



Ours

Figure 16. Examples of video frame prediction from UCF-101 dataset [38].



Frame 1

Frame 2

Frame 3 (ground-truth)



FlowNet2



Ours



Frame 1



Frame 2



Frame 3 (ground-truth)



FlowNet2



Ours

Figure 17. Examples of video frame prediction from UCF-101 dataset [38].